

## ARTICLE OPEN

## Computational discovery of p-type transparent oxide semiconductors using hydrogen descriptor

Kanghoon Yim<sup>1,3</sup>, Yong Youn<sup>1</sup>, Miso Lee<sup>1</sup>, Dongsun Yoo<sup>1</sup>, Joohee Lee<sup>1</sup>, Sung Haeng Cho<sup>2</sup> and Seungwu Han<sup>1</sup>

The ultimate transparent electronic devices require complementary and symmetrical pairs of n-type and p-type transparent semiconductors. While several n-type transparent oxide semiconductors like InGaZnO and ZnO are available and being used in consumer electronics, there are practically no p-type oxides that are comparable to the n-type counterpart in spite of tremendous efforts to discover them. Recently, high-throughput screening with the density functional theory calculations attempted to identify candidate p-type transparent oxides, but none of suggested materials was verified experimentally, implying need for a better theoretical predictor. Here, we propose a highly reliable and computationally efficient descriptor for p-type dopability—the hydrogen impurity energy. We show that the hydrogen descriptor can distinguish well-known p-type and n-type oxides. Using the hydrogen descriptor, we screen most binary oxides and a selected pool of ternary compounds that covers Sn<sup>2+</sup>-bearing and Cu<sup>1+</sup>-bearing oxides as well as oxychalcogenides. As a result, we suggest La<sub>2</sub>O<sub>2</sub>Te and CuLiO as promising p-type oxides.

npj Computational Materials (2018)4:17 ; doi:10.1038/s41524-018-0073-z

## INTRODUCTION

Transparent oxide semiconductors (TOSs) are electrically semi-conducting and have wide band gaps that make the material transparent to visible light. TOSs have great potentials in various applications like light-emitting diodes, solar cells, touch panels, and transparent thin film transistors.<sup>1–3</sup> If both n-type and p-type TOSs with good performances are available, it would empower transparent bipolar devices with high electrical efficiency.<sup>4,5</sup> However, while a multitude of n-type TOSs like ZnO and InGaZnO show good device performances, only a few p-type TOSs were identified and their electrical properties lag far behind those of n-type counterparts. For instance, SnO and Cu<sub>2</sub>O are well-known p-type oxides with appreciable conductivity, but they have stability issues<sup>6,7</sup> and transparency is poor in Cu<sub>2</sub>O. Since p-type conductivity was demonstrated for CuAlO<sub>2</sub>,<sup>8</sup> extensive studies revealed a series of p-type TOSs with delafossite structures such as CuM<sup>III</sup>O<sub>2</sub>, AgM<sup>III</sup>O<sub>2</sub> (M<sup>III</sup> = Sc, Cr, Co, Ga, In), as well as SrCu<sub>2</sub>O<sub>2</sub>, LaCuOSe, and Rh<sub>2</sub>ZnO<sub>4</sub>.<sup>9–15</sup> However, none of them has high conductivity and good transparency simultaneously; for p-type oxides whose hole conductivities are higher than 10 Sm<sup>-1</sup>, the transparencies are lower than 70%. On the contrary, the p-type oxides with excellent transparency have hole conductivities below 1 Sm<sup>-1</sup>.<sup>16</sup>

The fundamental reasons that underlie the scarcity of p-type transparent oxides are two-fold; first, valence bands of oxides are low in energy, and, therefore, holes are easily compensated by defects like oxygen vacancy and ubiquitous hydrogen, resulting in the low p-type dopability. Second, the valence band maximum (VBM) mainly consists of localized oxygen 2p orbitals, which leads to a large hole effective mass ( $m_h$ ). Such fundamental restrictions require searching over a large material space, which would be

prohibitively expensive and time consuming. Recently, several density functional theory (DFT) calculations attempted to discover new p-type transparent oxides that may surpass the limitation of known p-type oxides.<sup>17–20</sup> While transparency can be directly assessed by the optical band gap ( $E_g^{\text{opt}}$ ) in DFT calculations, the p-type conductivity is a quantity combining several physical properties like carrier density, scattering time, and effective mass, even within the simple Drude model. In the foregoing theoretical screening efforts,<sup>17–20</sup>  $m_h$  was used as a primary descriptor for p-type conductivity, and oxides were filtered through the condition  $m_h \leq 0.5–1.5 m_e$ . However, the low dopability is another critical factor as mentioned above. In ref. <sup>17</sup>, the p-type dopability was tested in terms of defect energies, but only for the candidate materials screened by  $m_h$  and  $E_g$ . To consider the dopability at the front, Sarmadian et al.<sup>19</sup> added the branch point energy (BPE) to the primary screening parameter together with  $m_h$ . In the complex band structure, BPE corresponds to the energy level at which the character of transient mid-gap states shifts from valence-like to conduction-like, resulting in the Fermi level pinning at this energy.<sup>21</sup> Therefore, BPE close to the valence edge may lead to facile p-type doping. In ref. <sup>19</sup>, BPE was calculated as the weighted average of the mid-gap energies over the Brillouin zone, which is sensitive to the curvature of valence and conduction bands.

The BPE and  $m_h$  are parameters that can be easily obtained from the DFT calculations on primitive cells, enabling high-throughput screening over more than thousands of oxides. However, their predictive power was not explicitly checked. In Fig. 1, we evaluate these two descriptors against metal oxides that are well known to be p-type or n-type experimentally. Some oxides can change the carrier type depending on the growth

<sup>1</sup>Department of Materials Science and Engineering and Research Institute of Advanced Materials, Seoul National University, Seoul 08826, Korea and <sup>2</sup>Electronics and Telecommunications Research Institute (ETRI), Daejeon 34129, Korea

Correspondence: Seungwu Han (hansw@snu.ac.kr)

<sup>3</sup>Present address: Korea Institute of Energy Research, Daejeon 34129, Korea

These authors contributed equally: Kanghoon Yim, Yong Youn.

Received: 13 November 2017 Revised: 27 February 2018 Accepted: 7 March 2018

Published online: 03 April 2018

condition and external dopants. The distinction given here is based on the more facile doping type. In Fig. 1, smaller  $m_h$  and lower BPE correspond to the criteria for good p-type oxides. However, it is seen that  $m_h$  and/or BPE fail to resolve the carrier type of the given material; many typical n-type oxides such as  $\text{SnO}_2$ ,  $\text{SrTiO}_3$ ,  $\text{ZnO}$ , and  $\text{TiO}_2$  also have relatively small  $m_h$  ( $1.5\text{--}2.5 m_e$ ) compared to several p-type oxides. In addition, BPEs of some p-type oxides ( $\text{Cu}_2\text{O}$ ,  $\text{CuGaO}_2$ , and  $\text{SrCu}_2\text{O}_2$ ) are close to the conduction bottom, rather than the valence top, and some n-type oxides ( $\text{TiO}_2$  and  $\text{Ta}_2\text{O}_5$ ) have lower BPEs compared to many p-type oxides. Most notably,  $\text{Ba}_2\text{BiTaO}_6$  and  $\text{SnNb}_2\text{O}_6$ , materials synthesized and tested for possible p-type conductivity, occupy the sweet spot in Fig. 1 but did not show any appreciable conductivity.<sup>18,22</sup> Therefore, it is concluded that neither  $m_h$  nor BPE is a reliable predictor in screening p-type transparent oxides.

Herein we propose a novel descriptor for p-type transparent oxides that uses the formation energy of hydrogen interstitial defect. We were motivated by ref.<sup>22</sup> showing that the Fermi level

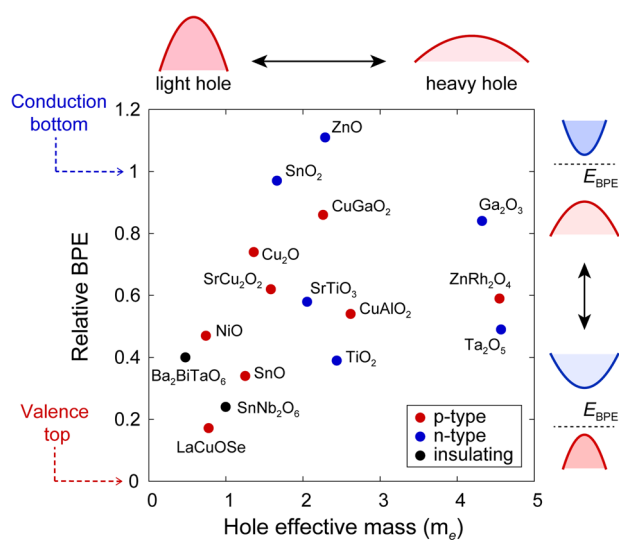


**Fig. 1** Hole effective mass and relative BPE ( $=[\text{BPE} - E_{\text{VBM}}]/E_g$ ) of archetypal p-type and n-type oxides. The electrical properties of  $\text{Ba}_2\text{BiTaO}_6$  [18] and  $\text{SnNb}_2\text{O}_6$  [22] were reported recently.

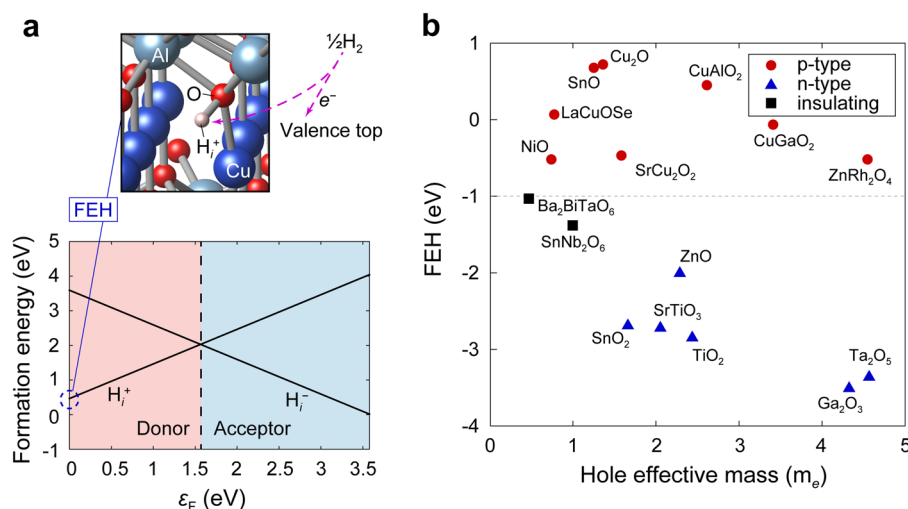


**Fig. 2** **a** Defect formation energy of  $\text{H}_i$  in  $\text{CuAlO}_2$  as a function of the Fermi level ( $\epsilon_F$ ). The vertical dashed line indicates the hydrogen transition level separating donor-like and acceptor-like hydrogen. The top figure shows the atomistic configuration of  $\text{H}_i^+$  in  $\text{CuAlO}_2$ . **b** FEH vs. hole effective mass of known p-type and n-type oxides presented in Fig. 1

position in  $\text{SnNb}_2\text{O}_6$  was correctly estimated by considering various point defects, implying that a proper p-type predictor should also take the defect chemistry into account. We note that the former screening studies<sup>17–19</sup> also calculated intrinsic defect energies to examine the p-type dopability but it was only for the finally screened materials. In addition, the full defect calculation used in those studies is highly expensive. The new descriptor suggested here is computationally efficient and can provide a well-defined decision boundary that can classify known p-type and n-type oxides. By conducting high-throughput screening using the new descriptor and  $m_h$ , we screen binary and ternary oxides, and identify promising p-type TOSs.

## RESULTS AND DISCUSSION

Formation energy of hydrogen interstitial defect as a new descriptor

We propose that the defect formation energy of hydrogen interstitial in +1 charge state ( $\text{H}_i^+$ ) with the Fermi level at the valence top (FEH hereafter) is a reliable descriptor for p-type oxides. Figure 2a shows the definition of FEH in the formation-energy diagram. (For convenience, the chemical potential of H is set to the half of  $\text{H}_2$  molecular energy.) The higher the FEH, the stronger the p-type dopability is. This can be rationalized as follows: first, hydrogen is universal and can actually compensate holes in experiment.<sup>23,24</sup> Second, in the present definition, hydrogen transfers an electron to the valence top that corresponds to the Fermi level, and therefore FEH correlates with the valence band position with respect to the vacuum. Figure 2a also shows the atomic sites of  $\text{H}_i^+$  in  $\text{CuAlO}_2$ , forming the O–H bond. Similar O–H bonds are found for other oxides as well.

Figure 2b shows FEH vs.  $m_h$  for the same oxides as in Fig. 1. It is striking that FEH can clearly distinguish the n-type and p-type oxides with the decision boundary at  $\text{FEH} = -1$  eV. Furthermore,  $\text{SnO}$  and  $\text{Cu}_2\text{O}$ , p-type oxides with good conductivity, rank high on the FEH scale. Interestingly, the insulating  $\text{Ba}_2\text{BiTaO}_6$  and  $\text{SnNb}_2\text{O}_6$  lie in the middle range of FEH. It is also noticeable that  $\text{ZnO}$  has the highest FEH among n-type oxides, recalling that  $\text{ZnO}$  can exhibit p-type conductivity by nitrogen doping.<sup>25,26</sup> The foregoing discussions support that FEH constitutes a good predictor of the conduction type in oxides. We note that FEH is a descriptor of inclination for p-type but a low FEH value does not necessarily mean that it is a good n-type oxide. In Fig. S1, we compare FEH

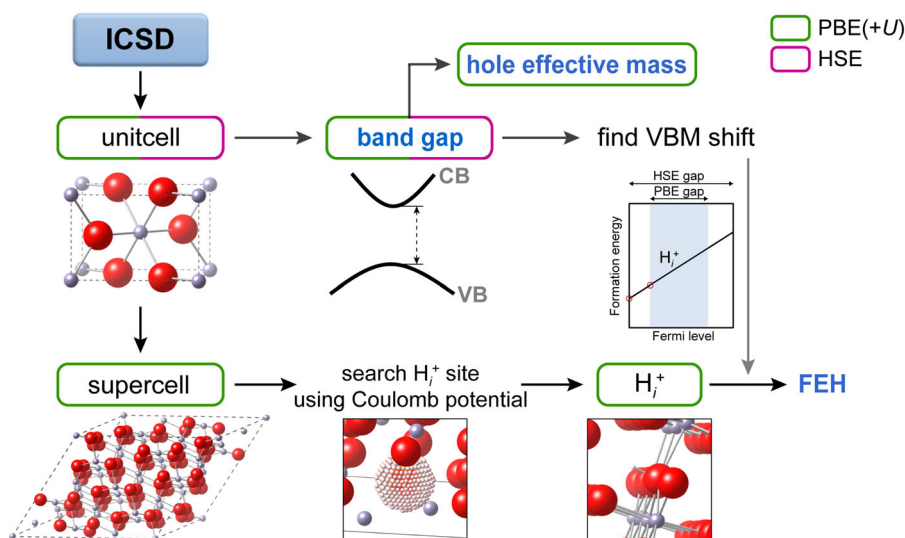


**Fig. 3** Schematic workflow for calculating FEH

with experimental ionization potential (IP), which shows a linear correlation between FEH and IP. This supports that FEH is an indicator for the VBM energy with respect to the vacuum level.

Using the hydrogen formation energy in assessing the dopability is reminiscent of the universal band alignment with respect to the H(+/-) level,<sup>27</sup> which also relates to the doping type. In Fig. S2, we compare FEH and H(+/-) level for some oxides. It is found that the two quantities correlate to some extent, but the H(+/-) level does not separate n-type and p-type tendency as clearly as FEH. In addition, computation of H(+/-) is more expensive than FEH.

#### Screening over binary oxides

We now use FEH in screening p-type oxides. To enable high-throughput screening of p-type TOSs, we develop an automation procedure to calculate the band gap, hole effective mass, and FEH, as depicted in Fig. 3 (see Methods section for more details). To be brief, the computation consists of crystalline and defect calculations; the crystalline calculations yield the effective mass with the PBE functional and the optical band gap ( $E_g^{\text{opt}}$ ) in one-shot hybrid calculation with the HSE functional.<sup>28</sup> This part also evaluates the relative shift in the valence top between PBE and HSE ( $\Delta\text{VBM}$ ) that will be used in correcting the band gap in the defect calculations (see below).<sup>29</sup> In the defect calculations, the initial positions of  $\text{H}_i^+$  are first selected using the Coulomb potential since  $\text{H}_i^+$  is essentially positively charged proton and its energy mainly depends on the electrostatic potential. The stable position of  $\text{H}_i^+$  is then obtained by relaxing the structure within PBE. To correct the band gap, we simply shift the valence edge using  $\Delta\text{VBM}$  obtained in the above. As shown in Fig. S3, this correction reproduces the full hybrid calculations with the root mean square error of 0.18 eV.

Through the automated procedure, we first conduct a high-throughput calculation for most binary oxides from Inorganic Crystal Structure Database (ICSD).<sup>30</sup> When polymorphism exists for specific compositions, we choose the structures whose total energies are within 10 meV/atom from the lowest value. Figure 4a shows FEH values and hole effective masses of binary oxides. The transparency of each data point is determined by  $E_g^{\text{opt}}$ ; the symbol is completely transparent for  $E_g^{\text{opt}} > 3.1$  eV and it becomes progressively opaque down to  $E_g^{\text{opt}} = 1.8$  eV. We posit that promising p-type oxides have  $\text{FEH} > -1$  eV since all known p-type oxides lie in this region (see Fig. 2b). In Fig. 4a, we cannot find

any new p-type candidates while every known p-type binary oxide (name in orange) is identified according to the present criterion.

#### Screening over ternary oxides

To discover new p-type oxides, we extend the search space to ternary oxides. Although the automation procedure is tuned for the high-throughput data production, defect calculations still require much longer computational time than for the crystalline calculations. Therefore, we restrict the ternary space by considering the known design principles of p-type oxides; first, many p-type oxides have valence states that have more delocalized character and higher position of VBM by hybridizing with cation orbitals. For example, in SnO,  $\text{Sn}^{2+}$  configuration have electronic configuration of  $4s^2$  that strongly hybridize with oxygen  $2p$  orbitals.<sup>31</sup> In the case of  $\text{Cu}_2\text{O}$  and  $\text{CuAlO}_2$ ,  $\text{Cu}^{1+}$  with  $3d^{10}$  configuration forms the valence top.<sup>32</sup> Another design principle for p-type can be inferred from  $\text{LaCuOSe}$  which records the highest conductivity to date.<sup>14</sup> Here, the large enhancement of p-type conductivity comes from  $\text{Se}^{2-}$  that raises the VBM energy and reduces effective hole mass owing to larger orbital size than  $\text{O}^{2-}$ .<sup>33</sup> In this respect, oxychalcogenides are also worth investigating. It must be noted that the delocalized and high valence states of oxychalcogenides are derived from the multi-anion character. If chalcogen atoms form polyanions, the compound usually has a VBM energy higher than for typical oxides. For example, FEH of Sn ( $\text{SO}_4$ ) is lower than for SnO (see Fig. 4).

From foregoing discussions, we choose  $\text{Sn}^{2+}$ -bearing and  $\text{Cu}^{1+}$ -bearing ternary oxides and ternary oxychalcogenides among ternary compounds. In addition, we consider only stable phases from the database obtained by our previous work.<sup>28</sup> As results, FEH's for 40 ternary compounds are calculated as presented in Fig. 4b. It is noticeable that every known p-type oxide (name in orange) including delafossite structures satisfies the condition of  $\text{FEH} > -1$  eV, reconfirming validity of the present descriptor. Figure 4b reveals several candidate p-type oxides that satisfy  $\text{FEH} > -1$  eV but have not been tested experimentally as far as we are aware. The detailed data for these materials are listed in Table 1. In Table 1, several non-delafossite candidate oxides are found among  $\text{Cu}^{1+}$ -bearing oxides in the form of  $\text{CuM}'\text{O}$  ( $M' = \text{Li}, \text{Na}, \text{K}, \text{Rb}, \text{Cs}$ ). All these compounds have the same symmetry ( $I4m2$ ) in their most stable phases except for  $\text{CuCsO}$  ( $Cmcm$ ), and they commonly include  $\text{Cu}^{1+}$  layers formed by closed  $\text{Cu}_4\text{O}_4$  four-membered rings (see Fig. 5a for  $\text{CuLiO}$ ). Among  $\text{CuM}'\text{O}$

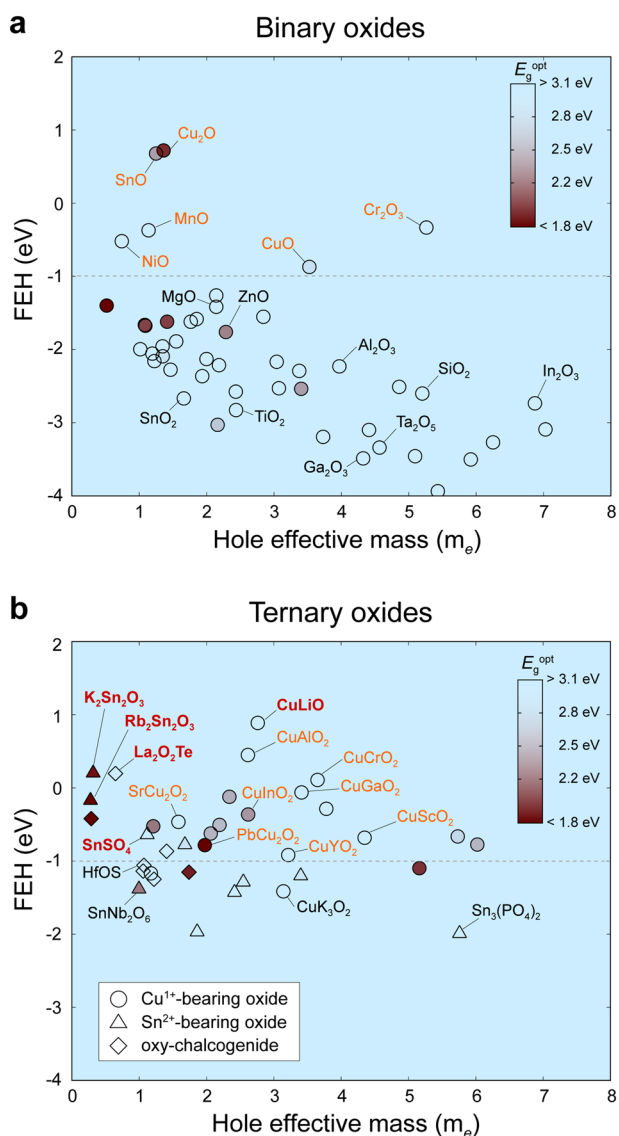


**Fig. 4** FEH and hole effective mass for **a** binary oxides and **b** ternary oxides. Promising p-type candidates and known p-type oxides are indicated in red-bold and orange, respectively. The transparency of each material is emulated by the optical band gap

compounds, CuLiO has the highest FEH value (0.89 eV), the highest among ternary oxides we explored. The enthalpy of formation of CuLiO from binary phases,  $\frac{1}{2}\text{Li}_2\text{O}$  and  $\frac{1}{2}\text{Cu}_2\text{O}$ , is  $-0.23$  eV, meaning that CuLiO is thermodynamically stable against phase separation. We note that the averaged  $m_h$  of CuLiO ( $2.76 m_e$ ) is slightly bigger than for CuAlO<sub>2</sub> ( $2.66 m_e$ ) but the valence band of CuLiO is more isotropic than CuAlO<sub>2</sub> (see Fig. 5b). From the defect calculation of CuLiO in Fig. 5c, we find that Li vacancy ( $V_{\text{Li}}$ ) is energetically more favorable than  $V_{\text{Cu}}$ , unlike delafossites in which  $V_{\text{Cu}}$  is regarded as the major acceptor. The calculated transition level of  $V_{\text{Li}}$  ( $0/-$ ) is  $0.24$  eV above VBM, which is shallower than Cu vacancies in known p-type oxides ( $0.4$ – $0.7$  eV).<sup>34,35</sup> Thus, with its facile formation, the intrinsic defect  $V_{\text{Li}}$  could lead to p-type doping in CuLiO without external dopants. FEH of other  $\text{CuM}'\text{O}$  compounds decreases with the increasing atomic number of  $M'$ .

Among  $\text{Sn}^{2+}$ -bearing oxides, only a few oxides could be classified as p-type according to the present criterion. All  $\text{Sn}^{2+}$ -bearing oxides have valence states mixed with  $\text{Sn-4s}^2$ , but they have lower FEH compared to SnO. This might be the effect of stronger interaction between the other cation and oxygen, which is also the origin of the larger band gap and better phase stability. Therefore, a trade-off between the band gap and p-type dopability may exist in  $\text{Sn}^{2+}$ -bearing oxides. The highest FEH values are found in  $\text{K}_2\text{Sn}_2\text{O}_3$  and  $\text{Rb}_2\text{Sn}_2\text{O}_3$ . In fact, these two materials were already suggested in the former high-throughput screening,<sup>17</sup> and expected to be good p-type oxides in our criterion, too. However, their small  $E_g^{\text{opt}}$  would be an obstacle against transparent applications. We suggest  $\text{SnSO}_4$  as a new p-type TSO since it has a wide band gap of  $5.12$  eV and small  $m_h$  of  $1.12 m_e$ . The crystal structure and defect formation energies of  $\text{SnSO}_4$  at oxygen-rich condition is provided in Fig. S5. As expected by relatively low FEH value ( $-0.8$  eV), the acceptors in  $\text{SnSO}_4$  partially compensated by the hydrogen interstitial defect, so the carrier concentration needs to be increased by external doping. It is noted that the oxides having polyanion groups like  $(\text{SO}_4)^{2-}$  and  $(\text{PO}_4)^{3-}$  tend to have lower FEH values as the polyanionic groups bring down VBM compared to typical oxides due to higher electronegativity. For example,  $\text{Sn}_3(\text{PO}_4)_2$  is not classified as p-type since it has low FEH.

For ternary oxychalcogenides, only a few oxides from ICSD contain negatively charged S, Se, and Te, as chalcogen elements usually exist in the form of polyanions rather than pure anions. Nevertheless, a promising candidate,  $\text{La}_2\text{O}_2\text{Te}$ , is found among oxychalcogenides.  $\text{La}_2\text{O}_2\text{Te}$  has the highest FEH value ( $0.2$  eV) among all wide gap ( $E_g^{\text{opt}} > 3$  eV) candidates and its  $m_h$  is also small ( $0.65 m_e$ ). The calculated enthalpy of formation of  $\text{La}_2\text{O}_2\text{Te}$  from binary oxides,  $\frac{1}{2}\text{La}_2\text{O}_3$  and  $\frac{1}{2}\text{La}_2\text{Te}_3$ , is  $-0.83$  eV per formula unit, confirming the stability. The crystal structure, electronic structure, and the defect formation energies of  $\text{La}_2\text{O}_2\text{Te}$  are given in Fig. 5d–f. The structure consists of alternating O and Te layers. Since VBM mainly consists of Te-5p states as shown in Fig. 5e, the hole conductivity is expected to be high along lateral directions on the Te layer. The defect formation energies in Fig. 5f confirms that  $\text{La}_2\text{O}_2\text{Te}$  would behave as p-type in the oxygen-rich condition. The major intrinsic acceptor is  $V_{\text{La}}\text{-2H}$  complex whose transition level of ( $0/-$ ) is  $0.13$  eV above VBM. As a possible external dopant, Ca could easily take up the La site ( $\text{Ca}_{\text{La}}$ ) owing to the similar ionic radius. In Fig. 5f,  $\text{Ca}_{\text{La}}^{1-}$  behaves as a shallow acceptor and its formation energy is even lower than  $(V_{\text{La}}\text{-2H})^{1-}$ . In passing, we note that  $\text{La}_2\text{SeO}_2$  suggested in ref.<sup>19</sup> as a promising p-type oxide has a FEH value of  $-1.25$  eV that does not meet the present criterion.

In summary, we screened binary oxides and ternary compounds covering  $\text{Cu}^{1+}$ -bearing oxides,  $\text{Sn}^{2+}$ -bearing oxides, and oxychalcogenides to discover promising p-type TOSs. As a new descriptor for p-type oxides, we used the formation energy of  $\text{H}_i^+$  with the Fermi level at VBM. We demonstrated that the suggested descriptor can classify the conduction type of well-known oxides, while hole effective mass and BPE, the favored descriptors so far, failed to distinguish majority carrier types. As a result of screening, we found many new candidate p-type oxides that have never been reported before. Considering FEH, band gap, and hole effective mass, we suggest  $\text{La}_2\text{O}_2\text{Te}$  as the best candidate material from the present study, while  $\text{SnSO}_4$  and CuLiO are also expected to be comparable to existing p-type TOSs. We expect our work will trigger the experimental verification of the suggested p-type oxides and contribute to realizing transparent and high-performance electronic devices.

**Table 1.** New p-type candidate oxides satisfying  $FEH > -1$  eV. The optical band gap and hole effective mass are also provided. ( $m_1, m_2, m_3$ ) are effective masses along the principal axis and  $m_{avg}$  is the harmonic average of them

Type	Name	FEH (eV)	Hole effective mass ( $m_e$ )		Optical band gap (eV)
			$m_{avg}$	( $m_1, m_2, m_3$ )	
Sn <sup>2+</sup> -bearing oxides	K <sub>2</sub> Sn <sub>2</sub> O <sub>3</sub>	0.20	0.32	(0.32, 0.32, 0.32)	1.89
	Rb <sub>2</sub> Sn <sub>2</sub> O <sub>3</sub>	-0.17	0.28	(0.36, 0.25, 0.25)	1.66
	SnSO <sub>4</sub>	-0.64	1.12	(0.67, 7.51, 0.94)	5.40
	Sn <sub>4</sub> O <sub>2</sub> F <sub>4</sub>	-0.78	1.68	(2.23, 1.18, 2.04)	3.05
Cu <sup>1+</sup> -bearing oxides	CuLiO	0.89	2.76	(2.59, 2.59, 3.22)	3.10
	CuNaO	0.08	9.01	(18.42, 18.41, 4.46)	2.96
	BaCu <sub>2</sub> O <sub>2</sub>	-0.12	2.34	(4.96, 4.96, 1.14)	2.75
	Cu <sub>2</sub> SO <sub>4</sub>	-0.29	3.78	(2.33, 4.43, 7.23)	3.19
	Cu <sub>2</sub> NaO <sub>2</sub>	-0.51	2.19	(9.11, 156.7, 0.80)	2.83
	CsCuO	-0.53	1.21	(7.68, 0.46, 5.54)	2.45
	Cu <sub>3</sub> PO <sub>4</sub>	-0.56	3.50	(2.16, 17.67, 2.96)	2.55
	Cu <sub>2</sub> LiO <sub>2</sub>	-0.62	2.06	(43.49, 1.40, 1.40)	2.79
	CuKO	-0.66	5.73	(18.93, 18.93, 2.39)	2.99
	CuRbO	-0.78	6.02	(2.03, 329.4, 329.3)	2.80
	Cu <sub>3</sub> VO <sub>4</sub>	-0.79	2.55	(2.70, 2.52, 2.45)	2.01
	Oxychalcogenides	La <sub>2</sub> O <sub>2</sub> Te	0.20	0.65	(1.05, 0.31, 2.25)
La <sub>4</sub> O <sub>4</sub> Se <sub>3</sub>		-0.42	0.29	(0.10, 488.0, 47.15)	1.68
Y <sub>2</sub> OS <sub>2</sub>		-0.87	1.41	(2.56, 0.82, 1.90)	3.67

## METHODS

### DFT calculations

Vienna Ab initio Simulation Package<sup>36</sup> is used for the DFT calculations. We employ the PBE functional<sup>37</sup> for the exchange-correlation energy of electrons. For 3d transition metal oxides, we applied the on-site Hubbard correction to 3d orbitals (PBE +  $U$  method) with parameters fitted to reproduce the experimental formation enthalpies of transition metal oxides.<sup>38</sup> The energy cutoff of the plane-wave basis and  $\mathbf{k}$ -point sampling over the first Brillouin zone are chosen to ensure the energy convergence of 10 meV/atom. For the hybrid calculation, we used the HSE functional<sup>39</sup> with the fixed fraction of the Fock exchange of 0.25.

### Band gap

We adopt the approach for band gap calculations from our previous high-throughput study.<sup>28</sup> First, we compute energy levels along the lines connecting the high-symmetry  $\mathbf{k}$ -points using PBE(+ $U$ ) functional and determine the  $\mathbf{k}$ -points corresponding to the valence top and the conduction bottom (both direct and indirect). Then, we carry out the hybrid functional calculation using the band-edge  $\mathbf{k}$ -points identified by PBE(+ $U$ ) to obtain theoretical  $E_g$  and  $E_g^{opt}$ .

### Hole effective mass

For the non-parabolic band structure, the effective mass should be averaged over the reciprocal space. The averaged effective mass tensor within the semiclassical theory is obtained as follows:

$$\langle (M^{-1})_{\alpha\beta} \rangle = \frac{\sum_n \int d\mathbf{k} \frac{\partial^2 \varepsilon_{n\mathbf{k}}}{\partial k_\alpha \partial k_\beta} f_{n\mathbf{k}}}{\sum_n \int d\mathbf{k} f_{n\mathbf{k}}}, \quad (1)$$

where  $M$  is the effective mass tensor,  $\varepsilon_{n\mathbf{k}}$  is the energy level, and  $f_{n\mathbf{k}}$  is the Fermi-Dirac distribution of holes when the Fermi level is at VBM. The numerical average in Eq. (1) can be done by sampling the Brillouin zone with fine meshes as was done in previous works.<sup>17</sup> However, this approach would be computationally expensive since it requires sampling tens of thousands  $\mathbf{k}$ -points to obtain the accurate hole effective mass. Noting that  $f_{n\mathbf{k}}$  is practically non-zero only near VBM, we evaluate Eq. (1) only around the local maximum points that are within 0.1 eV from VBM, using fine  $\mathbf{k}$ -point meshes. This approach speeds up the computation several times without sacrificing the accuracy compared to the dense sampling of the whole Brillouin zone. The hole effective mass ( $m_h$ ) is set to the harmonic

average of components along the principal axis that are obtained by diagonalizing the effective mass tensor.

### Branch point energy

At BPE, the character of the decaying mid-gap states changes from valence-like to conduction-like. BPE can be approximated by the averaged mid-gap energy.<sup>40</sup>

$$BPE = \frac{1}{2N_{\mathbf{k}}} \sum_{\mathbf{k}} \left[ \frac{1}{N_{CB}} \sum_i \varepsilon_{c_i}(\mathbf{k}) + \frac{1}{N_{VB}} \sum_j \varepsilon_{v_j}(\mathbf{k}) \right], \quad (2)$$

where  $N_{\mathbf{k}}$  is number of sampled  $\mathbf{k}$ -points,  $\varepsilon_{c(v)}$  is eigenvalue in the conduction (valence) band,  $N_{CB}$  and  $N_{VB}$  are the numbers of considered conduction and valence band, respectively. Following previous literature, we scale  $N_{VB}$  according to the number of valence electrons (without  $d$  electrons) in the unit cell and  $N_{CB}$  is set to the half of  $N_{VB}$ .<sup>40</sup> To address the band-gap underestimation in PBE functional, we rigidly shift the valence and conduction bands from PBE calculations using the VBM and CBM differences between PBE and HSE results.

### Formation energy of defects

The defect formation energy ( $E_{for}$ ) is calculated within the supercell approach using the following equation:

$$E_{for}(q) = E_{tot}(q) - E_{tot}(\text{perfect}) + \sum N_i \mu_i + q(\varepsilon_F + \varepsilon_{VBM}) + E_{corr}, \quad (3)$$

where  $q$  is the charge state,  $N_i$  and  $\mu_i$  are the number and chemical potential of the chemical species  $i$ ,  $\varepsilon_F$  is the Fermi energy with respect to the VBM energy ( $\varepsilon_{VBM}$ ), and  $E_{corr}$  is the correction energy to remove spurious electrostatic interactions among image charges in the repeated cells. A supercell is chosen such that the minimum distance between defects from adjacent periodic cell is longer than 10 Å, corresponding to the defect concentration less than 1 atomic %. For the defect calculations, only  $\Gamma$  point is sampled. For  $E_{corr}$ , we applied the FNV correction<sup>41</sup> that can generally apply to materials including anisotropic dielectric constant.<sup>42</sup> By using a relatively large supercell and applying the cell-size correction, we assume that the calculated  $E_{for}$  corresponds to the formation energy of the isolated defect.

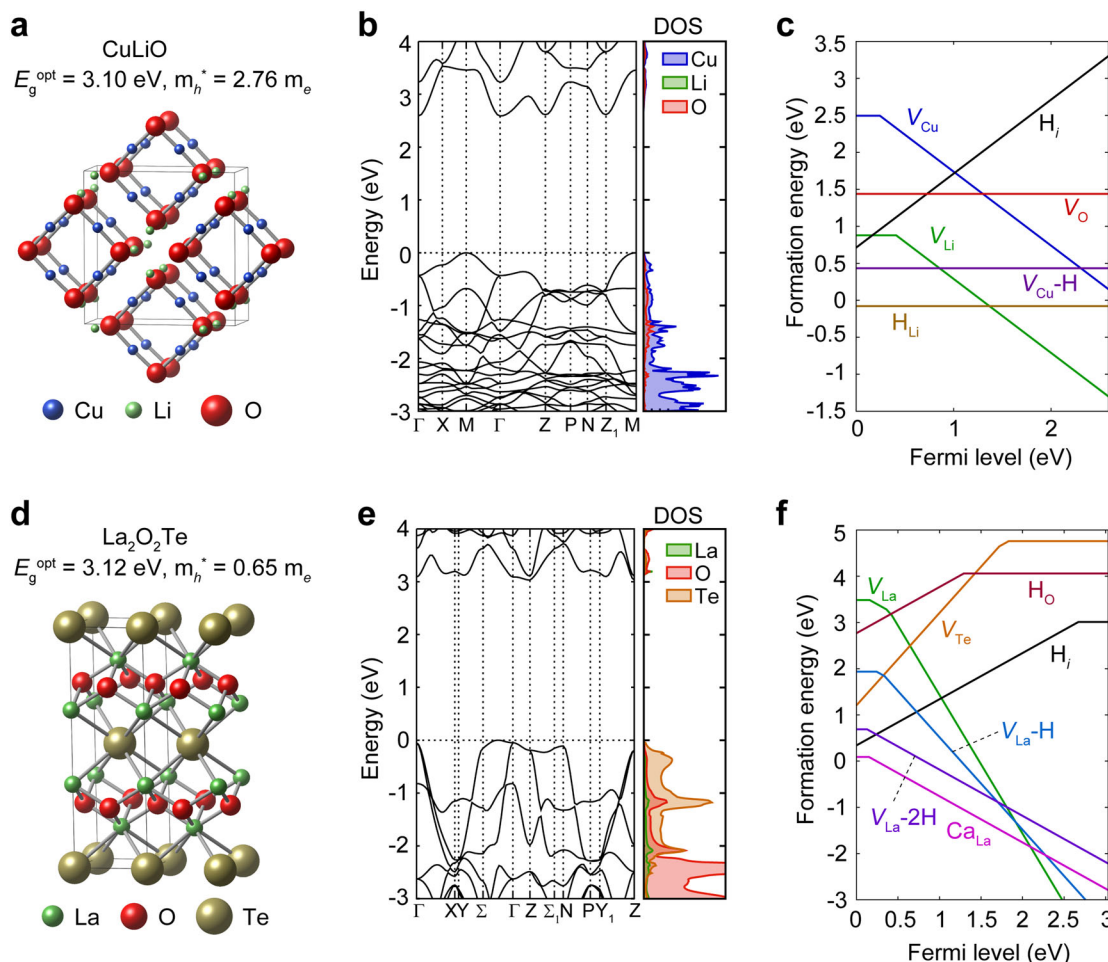


**Fig. 5** **a** The unit-cell structure of CuLiO. **b** Band structure and partial density of states. (The VBM is set to zero.) **c** The formation energies of intrinsic and hydrogen defects at the oxygen-rich condition. **d** Unit-cell structure of La<sub>2</sub>O<sub>2</sub>Te. **e** Band structure and partial density of states. (The VBM is set to zero.) **f** The formation energies of intrinsic and hydrogen defects at the oxygen-rich condition. For **b** and **e**, the GGA(+U) functional is used with scissor-correction to match with the HSE gap

### Hydrogen interstitial site

The systematic procedure to obtain FEH is schematically explained in Fig. 3. From the extensive test on H<sub>i</sub><sup>+</sup> in various oxides, we find that H<sub>i</sub><sup>+</sup> is always stable when it is bonded to oxygen with the bond length of ~1 Å. Furthermore, the O–H bond usually lies in the direction of the maximum Coulomb potential, which can be understood by the protonic nature of H<sub>i</sub><sup>+</sup>. To identify the stable sites of H<sub>i</sub><sup>+</sup> efficiently, we first choose initial positions of H<sub>i</sub><sup>+</sup> around oxygen based on the Coulomb potential. The position is then relaxed within PBE(+U). Since the Fermi level is at VBM, FEH significantly depends on the band gap. To overcome the band-gap underestimation in PBE, we further relax the structure and compute FEH using the HSE functional. Since the hybrid calculation is costly, we tried to identify a simple relationship between FEH calculated using the two functionals. Figure S3 shows a linear relation between FEH<sub>HSE</sub> and FEH<sub>PBE</sub> over a range of oxides. The fitting result is as follows:

$$\text{FEH}_{\text{HSE}} = \text{FEH}_{\text{PBE}} + \Delta\text{VBM} - 0.27 \text{ eV}, \quad (4)$$

where  $\Delta\text{VBM}$  is the difference in  $\epsilon_{\text{VBM}}$  between PBE(+U) and HSE calculation when aligned with respect to the common reference point.<sup>43</sup> ( $\Delta\text{VBM}$  is obtained from the unit-cell calculation.) The rigid shift of 0.27 eV in Eq. (4) can be explained by the over binding of O–H bond in PBE. Every FEH result in the present work is obtained by Eq. (4).

### Data availability

All data sets used in this work are available from the corresponding author on reasonable request.

### ACKNOWLEDGEMENTS

This work was supported by Electronics and Telecommunications Research Institute (ETRI) grant funded by the Korean government [17ZB1500, Development of oxide semiconductor materials, photonic integrated circuit, and packaging for high thermal dissipation] and Creative Materials Discovery Program through the National Research Foundation of Korea (NRF) funded by Ministry of Science and ICT (2017M3D1A1040689). The computation was carried out at the KISTI supercomputing center (KSC-2016-C3-0006).

### AUTHOR CONTRIBUTIONS

K.Y., Y.Y., M.L., D.Y., and J.L. developed in-house automation code. K.Y., Y.Y., and M.L. carried out the high-throughput calculation and analyzed the data. K.Y. and Y.Y. wrote the manuscript. S.C. reviewed and discussed the result. S.H. coordinated the whole work. All authors reviewed and commented on the manuscript.

### ADDITIONAL INFORMATION

**Supplementary Information** accompanies the paper on the *npj Computational Materials* website (<https://doi.org/10.1038/s41524-018-0073-z>).

**Competing interests:** The authors declare no competing interests.

**Publisher's note:** Springer Nature remains neutral with regard to jurisdictional claims in published maps and institutional affiliations.

## REFERENCES

- Fortunato, E., Barquinha, P. & Martins, R. Oxide semiconductor thin-film transistors: a review of recent advances. *Adv. Mater.* **24**, 2945–2986 (2012).
- Cui, J. et al. Indium tin oxide alternatives—high work function transparent conducting oxides as anodes for organic light-emitting diodes. *Adv. Mater.* **13**, 1476–1480 (2001).
- Varghese, O. K., Paulose, M. & Grimes, C. A. Long vertically aligned titania nanotubes on transparent conducting oxide for highly efficient solar cells. *Nat. Nanotech.* **4**, 592–597 (2009).
- Thomas, G. Materials science: invisible circuits. *Nature* **389**, 907–908 (1997).
- Grundmann, M. et al. Oxide bipolar electronics: materials, devices and circuits. *J. Phys. D Appl. Phys.* **49**, 213001 (2016).
- Caraveo-Frescas, J. A. et al. Record mobility in transparent p-type tin monoxide films and devices by phase engineering. *ACS Nano* **7**, 5160–5167 (2013).
- Engel, C. J., Polson, T. A., Spado, J. R., Bell, J. M. & Fillinger, A. Photoelectrochemistry of porous p-Cu<sub>2</sub>O films. *J. Electrochem. Soc.* **155**, F37–F42 (2008).
- Kawazoe, H. et al. p-Type electrical conduction in transparent thin films of CuAlO<sub>2</sub>. *Nature* **389**, 939–942 (1997).
- Nagarajan, R. et al. p-Type conductivity in the delafossite structure. *Int. J. Inorg. Mater.* **3**, 265–270 (2001).
- Tate, J. et al. p-Type oxides for use in transparent diodes. *Thin Solid Films* **411**, 119–124 (2002).
- Marquardt, M. A., Ashmore, N. A. & Cann, D. P. Crystal chemistry and electrical properties of the delafossite structure. *Thin Solid Films* **496**, 146–156 (2006).
- Sheets, W. C. et al. Silver delafossite oxides. *Inorg. Chem.* **47**, 2696–2705 (2008).
- Kudo, A., Yanagi, H., Hosono, H. & Kawazoe, H. SrCu<sub>2</sub>O<sub>2</sub>: a p-type conductive oxide with wide band gap. *Appl. Phys. Lett.* **73**, 220–222 (1998).
- Ueda, K. & Hosono, H. Band gap engineering, band edge emission, and p-type conductivity in wide-gap LaCuO<sub>5</sub><sub>1-x</sub>Se<sub>x</sub> oxychalcogenides. *J. Appl. Phys.* **91**, 4768–4770 (2002).
- Mizoguchi, H. et al. ZnRh<sub>2</sub>O<sub>4</sub>: a p-type semiconducting oxide with a valence band composed of a low spin state of Rh<sup>3+</sup> in a 4d<sup>6</sup> configuration. *Appl. Phys. Lett.* **80**, 1207–1209 (2002).
- Wager, J. F., Kezler, D. A. & Presley, R. E. *Transparent Electronics* 1st edn (Springer, New York, 2008).
- Hautier, G., Miglio, A., Ceder, G., Rignanese, G.-M. & Gonze, X. Identification and design principles of low hole effective mass p-type transparent conducting oxides. *Nat. Commun.* **4**, 2292 (2013).
- Bhatia, A. et al. High-mobility bismuth-based transparent p-type oxide from high-throughput material screening. *Chem. Mater.* **28**, 30–34 (2016).
- Sarmadian, N., Saniz, R., Partoens, B. & Lamoen, D. Easily doped p-type, low hole effective mass, transparent oxides. *Sci. Rep.* **6**, 20446 (2016).
- Cerqueira, T. F. T. et al. Identification of novel Cu, Ag, and Au ternary oxides from global structural prediction. *Chem. Mater.* **27**, 4562–4573 (2015).
- Demkov, A. A., Fonseca, L. R. C., Verret, E., Tomfohr, J. & Sankey, O. F. Complex band structure and the band alignment problem at the Si–high-k dielectric interface. *Phys. Rev. B* **71**, 195306 (2005).
- Katayama, S., Hayashi, H., Kumagai, Y., Oba, F. & Tanaka, I. Electronic structure and defect chemistry of tin(II) complex oxide SnNb<sub>2</sub>O<sub>6</sub>. *J. Phys. Chem. C* **120**, 9604–9611 (2016).
- Van De Walle, C. G. Hydrogen as a cause of doping in zinc oxide. *Phys. Rev. Lett.* **85**, 1012–1015 (2000).
- Kang, Y. et al. Hydrogen bistability as the origin of photo-bias-thermal instabilities in amorphous oxide semiconductors. *Adv. Electron. Mater.* **1**, 1400006 (2015).
- Lyons, J. L., Janotti, A. & Van de Walle, C. G. Why nitrogen cannot lead to p-type conductivity in ZnO. *Appl. Phys. Lett.* **95**, 252105 (2009).
- Reynolds, J. G. et al. Shallow acceptor complexes in p-type ZnO. *Appl. Phys. Lett.* **102**, 152114 (2013).
- Van de Walle, C. G. & Neugebauer, J. Universal alignment of hydrogen levels in semiconductors, insulators and solutions. *Nature* **423**, 626–628 (2003).
- Yim, K. et al. Novel high-κ dielectrics for next-generation electronic devices screened by automated ab initio calculations. *NPG Asia Mater.* **7**, e190 (2015).
- Park, S., Lee, B., Jeon, S. H. & Han, S. Hybrid functional study on structural and electronic properties of oxides. *Curr. Appl. Phys.* **11**, s337–s340 (2011).
- FIZ Karlsruhe. Inorganic crystal structure database. <http://icsd.fiz-karlsruhe.de>.
- Quackenbush, N. F. et al. Origin of the bipolar doping behavior of SnO from X-ray spectroscopy and density functional theory. *Chem. Mater.* **25**, 3114–3123 (2013).
- Raebiger, H., Lany, S. & Zunger, A. Origins of the p-type nature and cation deficiency in Cu<sub>2</sub>O and related materials. *Phys. Rev. B* **76**, 045209 (2007).
- Scanlon, D. O., Buckeridge, J., Catlow, C. R. A. & Watson, G. W. Understanding doping anomalies in degenerate p-type semiconductor LaCuOSe. *J. Mater. Chem. C* **2**, 3429–3438 (2014).
- Scanlon, D. O., Morgan, B. J. & Watson, G. W. Modeling the polaronic nature of p-type defects in Cu<sub>2</sub>O: the failure of GGA and GGA + U. *J. Chem. Phys.* **131**, 124703 (2009).
- Huang, D. & Pan, Y. First-principles calculations of intrinsic defects in the p-type semiconductor CuAlO<sub>2</sub>. *Can. J. Phys.* **88**, 927–932 (2010).
- Kresse, G. & Hafner, J. Ab initio molecular dynamics for liquid metals. *Phys. Rev. B* **47**, 558–561 (1993).
- Perdew, J. P., Burke, K. & Ernzerhof, M. Generalized gradient approximation made simple. *Phys. Rev. Lett.* **78**, 1396 (1997).
- Wang, L., Maxisch, T. & Ceder, G. Oxidation energies of transition metal oxides within the GGA + U framework. *Phys. Rev. B* **73**, 195107 (2006).
- Heyd, J., Scuseria, G. E. & Ernzerhof, M. Hybrid functionals based on a screened Coulomb potential. *J. Chem. Phys.* **118**, 8207–8215 (2003).
- Schleife, A., Fuchs, F., Rödl, C., Furthmüller, J. & Bechstedt, F. Branch-point energies and band discontinuities of III-nitrides and III-/II-oxides from quasiparticle band-structure calculations. *Appl. Phys. Lett.* **94**, 012104 (2009).
- Freysoldt, C., Neugebauer, J. & Van De Walle, C. G. Fully ab initio finite-size corrections for charged-defect supercell calculations. *Phys. Rev. Lett.* **102**, 016402 (2009).
- Kumagai, Y. & Oba, F. Electrostatics-based finite-size corrections for first-principles point defect calculations. *Phys. Rev. B* **89**, 195205 (2014).
- Alkauskas, A., Broqvist, P. & Pasquarello, A. Defect energy levels in density functional calculations: alignment and band gap problem. *Phys. Rev. Lett.* **101**, 046405 (2008).



**Open Access** This article is licensed under a Creative Commons Attribution 4.0 International License, which permits use, sharing, adaptation, distribution and reproduction in any medium or format, as long as you give appropriate credit to the original author(s) and the source, provide a link to the Creative Commons license, and indicate if changes were made. The images or other third party material in this article are included in the article's Creative Commons license, unless indicated otherwise in a credit line to the material. If material is not included in the article's Creative Commons license and your intended use is not permitted by statutory regulation or exceeds the permitted use, you will need to obtain permission directly from the copyright holder. To view a copy of this license, visit <http://creativecommons.org/licenses/by/4.0/>.

© The Author(s) 2018